

# Deeply supervised neural network with short connections for retinal vessel segmentation

Song Guo, Yingqi Gao, Kai Wang, Tao Li

No Institute Given

**Abstract.** The condition of vessel of the human eye is a fundamental factor for the diagnosis of ophthalmological diseases. Vessel segmentation in fundus image is a challenging task due to low contrast, the presence of microaneurysms and hemorrhages. In this paper, we present a multi-scale and multi-level deeply supervised convolutional neural network with short connections for vessel segmentation. We use short connections to transfer semantic information between side-output layers. Forward short connections could pass low level semantic information to high level and backward short connections could pass much structural information to low level. In addition, we propose using a structural similarity measurement to evaluate the vessel map. The proposed method is verified on DRIVE dataset and it shows superior performance compared with other state-of-the-art methods. Specially, with patch level input, the network gets 0.7890 sensitivity, 0.9803 specificity and 0.9802 AUC. Code will be made available at <https://github.com/guomugong/sdsn>. ...

**Keywords:** vessel segmentation, fundus image analysis, deeply supervised convolutional network, short connections

## 1 Introduction

Retinal fundus image analysis is key for ophthalmologists to deal with the diagnosis, screening and treatment of cardiovascular and ophthalmologic diseases, such as age-related fovea degeneration, diabetic retinopathy, glaucoma, hypertension, arteriosclerosis and choroidal neovascularization[1]. These diseases could lead to blindness if left untreated. Vessel segmentation is a basic step for the quantitative analysis of retinal images which is helpful to diabetic retinopathy[2] and locating of foveal region[3].

In clinical practice, manual annotation of blood vessels in retinal images is tedious, time-consuming and experienced[4]. Therefore, automated retinal vessel segmentation is necessary to reduce the annotation time. However, vessel segmentation is a challenging problem because of the following reasons[5]. 1) The size, shape and intensity level of retinal vessels vary hugely in different local areas. 2) The width of a vessel often ranges from 1 to 20 pixels, depending on both the width of vessel and the image resolution. Recognition of 1 pixel width micro-vessel is much difficult. 3) Other structures with similar intensity level may complicate the segmentation task, such as striped hemorrhage. Therefore,

the automated segmentation of retinal blood vessels has attracted significant attention over recent decades[6]. The existing segmentation algorithms could be divided into two categories: unsupervised and supervised methods[7].

1) Unsupervised Methods: The unsupervised methods can be divided into three subcategories: matched filtering, vessel tracking, and model-based algorithms. The matched filtering method[8] convolves a 2-D kernel with the retinal image and the matched filter response indicates the presence of the feature. To design the matched filter kernel, this method exploits the piece-wise linear approximation, the decrease in vessel diameter along vascular length, and the Gaussian-like intensity profile of retinal blood vessels. Vessel tracking algorithms[9] use local information to segment a vessel between two points. The center of the longitudinal cross-section of a vessel is determined by gray-level intensity and tortuosity. This method can provide accurate vessel width, but they are often unable to detect vessel segments that have no seed points. The model-based methods include the vessel profile models[10], active contour models[11], level sets based geometric models[12], and cluster algorithms[13].

2) Supervised Methods: Since unsupervised methods take vessel segmentation task without using any label related information, supervised methods show some advantages over unsupervised methods[6]. Supervised methods can be regarded as a pixel-level binary classification problem. Each pixel belongs to vessel or non-vessel. Supervised methods can be divided into three subcategories: pixel-level methods, patch-level methods, and image-level methods. The pixel-level methods[14], [15], [16] use a pixel-wise classifier to determine what it belongs to. The class label of each pixel is predicted by providing a square window, called a patch, centered on that pixel as an input. For example, Liskowski[15] adopts a deep convolutional neural network to classify vessel pixels and non-vessel pixels. Obviously, pixel-level methods are time-consuming and difficult to clinical requirements when dealing with large-scale retinal images. In some sense, vessel recognition can be regarded as a semantic segmentation problem. The usual segmentation methods consist of patch-level and image-level methods. The input of patch-level segmentation methods is a patch, and the output is a vessel map. We obtain the final segmentation result of a retinal image by puzzling the patch vessel map together, just like that did in [17], [18], [19]. What's more, the introducing of hyper-parameter patch size and the split of raw retinal images make patch-level methods much more complicated and time-consuming compared with image-level methods. Image-level methods[20], [21], [7] take a retinal image as input and it could produce a vessel map directly for only one forward pass. When considering the clinical application, the image-level methods have natural advantage over patch-level and pixel-level methods in time overhead. [7] uses HED[22] which is a FCN[23]-based edge detection network for image-level vessel segmentation. [21] designs a deep neural network DeepVessel based on HED and conditional random field, and the DeepVessel achieves state-of-the-art performance.

To address the inefficiency of pixel-level methods, we propose a deeply supervised fully convolutional neural network with short connections (S-DSN) that

fuses multi-level features together to obtain precise segmentation results. Within a single forward propagation, the network can produce a vessel probability map which is the same size as the original retinal image. Meanwhile, we use short connections between side-output layers to pass low level detail information to high level side-output layers. What's more, the structural information of high level side-output layer is as well passed back to low level layer. Extensive experiments on DRIVE dataset demonstrate the competitive performance of S-DSN. Specially, with image-level input, S-DSN achieves 0.9547 accuracy, 0.9793 AUC, 0.7893 sensitivity, 0.9789 specificity, 0.7843 s-measure. And with patch-level input, S-DSN achieves 0.9560 accuracy, 0.9802 AUC, 0.7890 sensitivity, 0.9803 specificity, 0.7980 s-measure.

The contributions of this paper are as follows. 1) We propose a deeply supervised fully convolutional neural network with short connections (S-DSN) for vessel segmentation. 2) We propose using a structural similarity measurement to evaluate the segmentation map. 3) We achieve the best comprehensive performance on DRIVE dataset.

The remainder of this paper is organized as follows. In Section 2, we describe the idea and principle of the S-DSN model. Experiments and analyses will be demonstrated in Section 3. Section 4 concludes the paper.

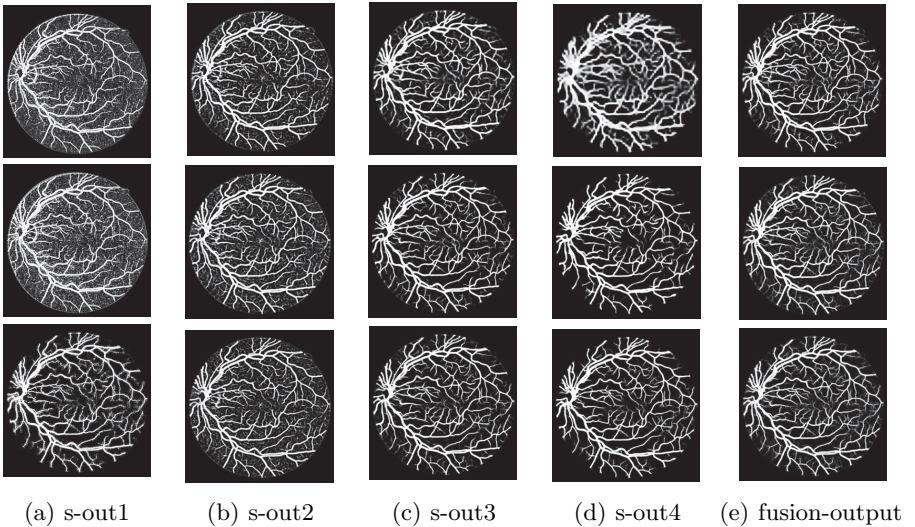


**Fig. 1.** Vessel segmentation results of side-output(s-out) layers produced by three networks. From top to bottom the network is normal DSN (with no short connections), FS-DSN (DSN with forward short connections), S-DSN (DSN with forward and backward short connections), respectively.

## 2 Deeply Supervised Neural Network with Short Connections (S-DSN)

As pointed out in most previous work[22], [23], a good semantic segmentation network should learn multi-level features. Further, it should have multiple stages with different receptive fields to learn more inherent features from different scales. FCN, taken as an example, uses skip connections to fusion multiple stages outputs, as well as the HED network, in which a series of side-output layers are added after each stage in VGGNet[24]. The HED network is first proposed for edge detection, but further several searchers use it for image-level vessel segmentation task[7], [21], and it shows significant performance. However, our experimental results show that such a network architecture is not appropriate for vessel segmentation directly. Fig. 1 provides such an illustration. Reasons for this phenomenon are straightforward. On one hand, the side-output of the first layer often contains too much noise. On the other hand, the features produced by the last side-output layer are too coarse because of the information loss of pooling operation.

To overcome the aforementioned problem, we propose a deeply supervised neural network with short connections for vessel segmentation. The overview of the S-DSN is illustrated in Fig. 2. The following subsections will describe the S-DSN in details.

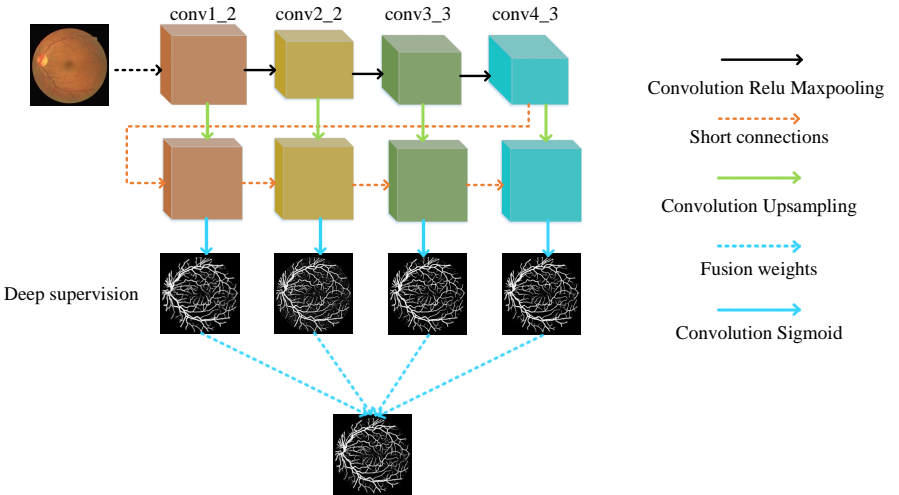


Fig. 2. An overview of proposed S-DSN.

## 2.1 HED for Vessel Segmentation

HED is an image-to-image edge detection network by means of fully convolutional neural network and deeply supervised nets[25]. [7] and [21] use HED for vessel segmentation. Fig. 3 gives an illustration of HED architecture and S-DSN.

Let  $S = \{(X_n, Y_n), n = 1, \dots, N\}$ , where  $X_n = \{x_j^{(n)}, j = 1, \dots, |X_n|\}$  denotes the raw input retinal image and  $Y_n = \{y_j^{(n)}, j = 1, \dots, |X_n|\}$ ,  $y_j^{(n)} \in \{0, 1\}$  denotes the corresponding ground truth binary vessel map for image  $X_n$ . Since we handle each image independently, we subsequently omit the subscript  $n$  for national convenience. For convenience, we denote the collection of all convolutional layers parameter of the standard network as  $W$ , and suppose there are  $M$  side-output layers in the network. Each side-output layer can be regarded as a stand-alone image-level classifier, in which the corresponding weights are denoted as  $w = (w^{(1)}, \dots, w^{(M)})$ . The objective function of the side-output layer is formulated as:

$$L_{side}(W, w) = \sum_{m=1}^M \alpha_m l_{side}^{(m)}(W, w^{(m)}) \quad (1)$$

where  $\alpha_m$  is the weight of the  $m$ -th side-output layer,  $l_{side}^{(m)}$  denotes the image-level loss function for side-output  $m$ . Since the distribution of vessel/non-vessel pixels is heavily biased: nearly 90% of the pixels are non-vessel for a retinal image, thus a class-balanced cross-entropy loss function is used.

$$l_{side}^{(m)}(W, w^{(m)}) = -\frac{|Y_-|}{|Y|} \sum_{j \in Y_+} \log Pr(y_j = 1|X; W, w^{(m)}) \quad (2)$$

$$- \frac{|Y_+|}{|Y|} \sum_{j \in Y_-} \log Pr(y_j = 0|X; W, w^{(m)}) \quad (3)$$

where  $|Y_-|$  and  $|Y_+|$  denote the non-vessel and vessel pixels in the ground truth  $Y$ .  $Pr(y_j = 1|X; W, w^{(m)})$  is computed by sigmoid function.

To utilize each side-output vessel probability map, a weight-fusion layer is adopted. The fusion output  $Y_{fuse}$  is defined as:

$$Y_{fuse} = \sigma\left(\sum_{m=1}^M h_m Y_{side}^{(m)}\right) \quad (4)$$

where  $\sigma(\cdot)$  is the sigmoid function,  $h_m$  is the fusion weight, and  $Y_{side}^{(m)}$  is the vessel probability map of side-output  $m$ . The side-output loss functions and the fusion-weight layer loss function are optimized together by back-propagation algorithm.

## 2.2 Short Connections

With the deepening of HED network, the receptive field of each side-output layer gets larger, which makes the corresponding vessel map much obscurer as observed

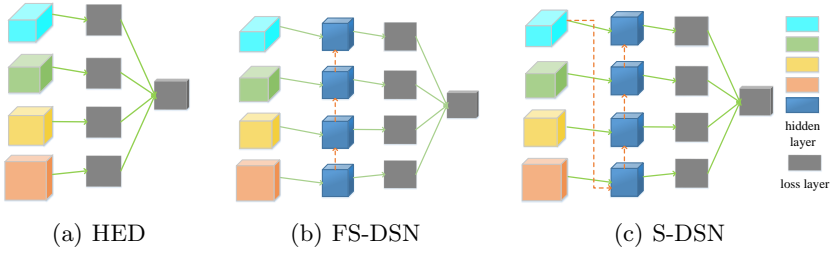


**Fig. 3.** Network architectures of HED and S-DSN. (a) HED with four side-output layers (b) FS-DSN (DSN with forward short connections) (c) S-DSN (DSN with forward and backward short connections)

in Fig. 1, especially for side-output 4. These observations inspired us to pass low level fine semantic information to high levels to alleviate the obscure situation. At the same time, we observe the vessel map generated by the first side-output layer contains too much noise while the map generated by the last side-output layer could capture the main vessel structure. Therefore, we propose delivering high level structural information to the first side-output layer to reduce its noise.

We adopt short connections to deliver semantic information just as shown in Fig. 4. The short connections consist of two parts: forward short connections and backward short connection. Forward short connections are among conv1\_2.16, conv2\_2.16, conv3\_3.16 and conv4\_3.16. Backward short connection is directed by conv4\_3 to conv1\_2.16. The implementation of short connections is based on  $1 \times 1$  convolutional kernel and concatenate operation provided by Caffe[26]. For backward short connection, we make a convolution operation with kernel size  $1 \times 1$  on conv4\_3, and the obtained feature map is concatenated with conv1\_2.16. For forward short connections, we make a convolution operation with kernel size  $1 \times 1$  on conv1\_2.16 and the obtained feature map is further concatenated with conv2\_2.16 to obtain conv2\_2.17. The information obtained from conv2\_2.17 is passed to conv3\_3.16 to get conv3\_3.17, and the information obtained from conv3\_3.17 is passed to conv4\_3.16.

### 2.3 Supervision

As we know, it's hard to optimize a deep neural network[27]. To alleviate the gradient vanish problem and to obtain the wanted vessel map, we use deep supervision information in our network. Next, we will describe the implementation detail of supervision for the second side-output. Supervision of other side-output layers shares the same procedure. We can see in Fig. 4, after the concatenation operation between conv2\_2.16 and the feature map delivered from conv1\_2.16, we get conv2\_2.17. Further, we perform convolutional operation with kernel size  $1 \times 1$  and sigmoid transformation for conv2\_2.17 sequentially to obtain a vessel map. The vessel probability map is compared with the ground truth and the loss of the second side-output layer is obtained.

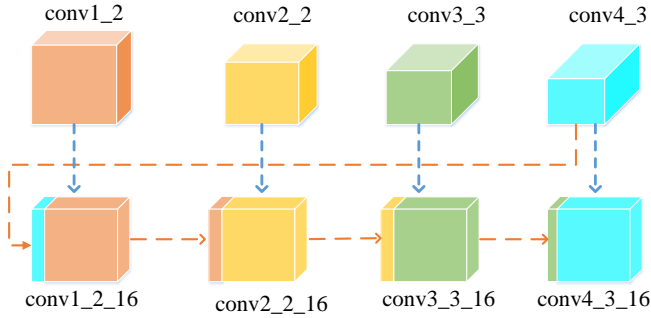


**Fig. 4.** An illustration of short connections.

## 2.4 Testing

When it comes to testing phase, given a retinal image, both side-output layers and weighted-fusion layer produce a vessel probability map. The output of weighted-fusion layer often regarded as the final vessel segmentation result because it fuses multi-scale vessel map together. The output of S-DSN is defined as:

$$Y_{S-DSN} = Y_{fuse} = \sigma\left(\sum_{m=1}^M h_m Y_{side}^{(m)}\right) \quad (5)$$

We set  $M$  equals 4 in our experiments. The meanings of the parameters in the above formula are the same as those of the Equ. 4.

## 3 Experimental Evaluation

The following subsections will describe the dataset we used, the evaluation criteria for vessel segmentation, the implementation and training details of the S-DSN, the experimental results and analyses at last.

### 3.1 Dataset

We evaluate our method on a publicly available retinal image vessel segmentation dataset: DRIVE. The DRIVE (Digital Retinal Images for Vessel Extraction)[28] dataset consists of 40 color fundus photographs. The set of 40 images has been divided into a training set and a test set, both containing 20 images. For the training images, a single manual segmentation of the vasculature is available. For the test cases, two manual segmentations are available; one is used as the gold standard, the other one can be used to compare computer generated segmentations with those of an independent human observer. For each image in DRIVE, a binary mask for FOV area is provided.

### 3.2 Details of Training

**Data Augmentation** As there are too fewer training images compared with the model complexity, training set augmentation methods are adopted. We used various transformations to augment the training set, including rotation by an angel of 90, 180 and 270, flipping horizontally and vertically, and scaling by a factor of 0.5 and 0.8.

**Model Implementation** We build the S-DSN architecture based on a publicly available convolutional network framework Caffe. Short connections of the S-DSN can be directly implemented by using the concatenate layer in Caffe.

**Parameter Settings** We fine-tune our network on VGGNet with learning rate  $1e-8$ , weight decay 0.0005 and momentum 0.9. Since the fine retinal vessel is merely one pixel width, which is too thin to respond in the high layers, thus we take four side output layers. The network is trained for 50000 iterations and the learning rate decreases by a factor of 10 after 25000 iterations. For forward short connections, one feature map generated from low layer is concatenated to high layer. For the backward short connection, two feature maps generated from conv4\_3 are concatenated to conv1\_2\_16. When training, for image-level S-DSN, the input is raw retinal images, and the output is the corresponding vessel probability maps, no pre-process or post-process is performed. For patch-level S-DSN, we split the raw retinal image into 9 patches, each of which is  $1/4$  size of the raw image. Further, the patches are upsampled  $2\times$ . At last, the patches are as input to the patch-level input S-DSN. When testing, we down-sample 9 patches  $2\times$  and further piece them into an image.

**Running Environment** The experimental platform is a PC equipped with an Intel Core i7 processor with eight 3.4GHZ cores, 18GB memory and NVIDIA Tesla K40c GPU, and the operating system is Ubuntu 16.04. It takes about 10 hours to train our model and about 0.4s to generate the final vessel map for image-level input.

### 3.3 Evaluation Criteria

**Non-Structure-Measurements** In vessel segmentation task, each pixel belongs to vessel or non-vessel. By comparing the segmentation results with ground truth, we employ four evaluation criteria, including the area under the roc curve (AUC), sensitivity (SE), specificity (SP), accuracy (ACC). The evaluation measurements are calculated only for pixels inside the FOV area. The SE, SP, ACC are defined as

$$SE = \frac{TP}{TP + FN}, SP = \frac{TN}{TN + FP}, ACC = \frac{TP + TN}{TP + FN + TN + FP} \quad (6)$$



where the true positives (TP) are vessel pixels that classified correctly, false negatives (FN) are vessel pixels that incorrectly classified as non-vessel, true negatives (TN) are non-vessel pixels that classified correctly, and false positives (FP) are non-vessel pixels that incorrectly classified as vessel pixels. The calculation of the SE, SP, ACC measurements is dependent on the threshold of the vessel probability map, but the AUC value takes into account of the fixed threshold. The ROC is plotted with the SE versus (1-SP) by varying the threshold. The perfect classifier gets AUC value equals to 1.

**Structure-Measurement** Obviously, the overall structure of the blood vessel is more important than the pixels correctness in evaluating the results of blood vessel segmentation in the fundus image. However, the SE, SP, ACC, AUC measures are all based on pixel-wise errors and they ignore the global structural similarities. We propose using a structural similarity measure (s-measure)[29] to evaluate the similarity between a vessel probability map and a ground-truth map, and s-measure shows superiority over AUC on 5 benchmark datasets. The s-measure is formulated as,

$$S = \alpha * S_o + (1 - \alpha) * S_r \quad (7)$$

where  $\alpha \in [0, 1]$ ,  $S_o$  is object-aware structural similarity and  $S_r$  is region-aware structural similarity. The region-aware structural similarity aims to capture object-part structure information without any special concern about complete foreground. The object-aware structural similarity is designed to mainly capture the structure information of the complete foreground objects. We use  $\alpha = 0.5$  in practice.

### 3.4 Results

**Vessel Segmentation Results of S-DSN** To show the effectiveness of proposed short connections, we perform experiments on three different DSN architectures, namely DSN with no short connections, DSN with forward short connections and DSN with both forward and backward short connections. The comparison of statistical measures of three DSN architectures are shown in Table 1, and Fig. 5 shows the subtle difference among three different DSN architectures. We can observe from Table 1 that FS-DSN behaves better than normal DSN in SE, SP, ACC, AUC, s-measure, and the S-DSN with extra backward short connections could further improve the performance compared with FS-DSN. In addition, we can observe from Fig. 1 that the side-output1 and side-output4 of S-DSN is much accurate compared with those of normal DSN. We could also observe from Fig. 5 that vessel segmentation result of normal DSN is much thicker compared with that of S-DSN, and this observation validates the effectiveness of the short connections which may lead the segmentation results of side-outputs more accurate. We conclude that S-DSN can alleviate the over-segmentation problem existed in the normal DSN.

**Table 1.** Performance comparison of vessel segmentation results of different image-level DSN architectures on DRIVE test set (best results are shown in bold).

Architecture	SE	SP	ACC	AUC	s-measure
DSN (no short connections)	0.7725	0.9793	0.9529	0.9775	0.7674
FS-DSN (Fig. 3(b))	0.7756	0.9802	0.9542	0.9788	0.7777
S-DSN (Fig. 3(c))	<b>0.7893</b>	0.9789	<b>0.9547</b>	<b>0.9793</b>	<b>0.7843</b>

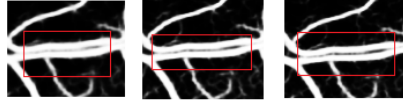


**Fig. 5.** Segmentation results of coarse vessel for three DSN architectures. (From left to right) Normal DSN, FS-DSN, S-DSN.

The segmentation results of image-level input S-DSN and patch-level input S-DSN are shown in Fig. 6. We can observe from Fig. 6 that vessel segmentation results of patch-level input S-DSN look more clear, and this observation corresponds to much higher SP of patch-level S-DSN. What’s more, patch-level input S-DSN achieves much higher specificity, accuracy, AUC, s-measure values than image-level input S-DSN as shown in Table 2.

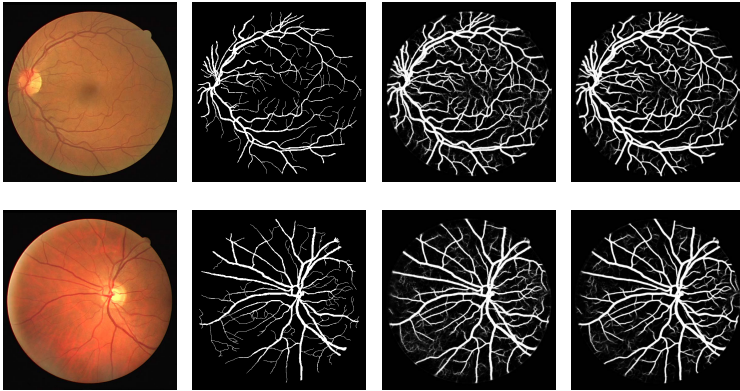


**Fig. 6.** (From left to right) retinal images, ground truth, vessel segmentation result of image-level input S-DSN, vessel segmentation result of patch-level input S-DSN.

**Comparing with Other Methods** In Table 2, we compare our approach with other state-of-the-art methods in terms of sensitivity, specificity, accuracy,

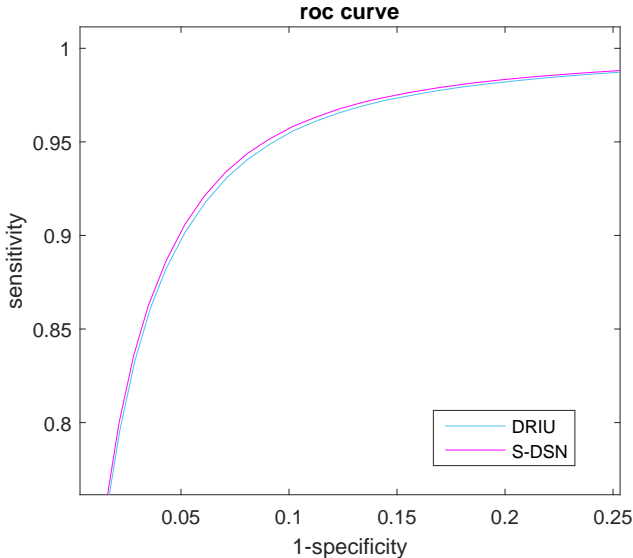


**Fig. 7.** Receiver Operating Characteristic (ROC) curve for DRIU and patch-level S-DSN on DRIVE dataset.

AUC, and s-measure on the DRIVE database. Our patch-level S-DSN achieves the best performance than the state-of-the-art methods regarding the sensitivity, accuracy, and AUC score. Especially, our patch-level S-DSN model achieves AUC score of 0.9802, while the existing best AUC score is 0.9793. In addition, our patch-level S-DSN has improved on all five measurements over DRIU, and the comparison of ROC curve is shown in Fig. 7. Compared with Feng[19], both our image-level S-DSN and patch-level S-DSN achieve higher sensitivity and AUC score. What’s more, as for F1 score, the patch-level S-DSN equals 0.8242 compared with 0.8183 in Feng.

## 4 Conclusion

In this paper, we propose a deeply supervised fully convolutional neural network with short connections, called S-DSN, for retinal vessel segmentation application. We use short connections to alleviate the semantic gap between side-outputs, and experimental results showed the effectiveness of short connections. In addition, we propose using a structural similarity metric for evaluating vessel map instead of only considering pixel-wise errors. We have shown that our method produces the best comprehensive result on a publicly available dataset DRIVE.

**Table 2.** Performance comparison of vessel segmentation results on the DRIVE test set (best results are shown in bold).

Methods	Year	SE	SP	ACC	AUC	s-measure
2nd human expert	-	0.7796	0.9717	0.9470	N.A	<b>0.8380</b>
Wavelets[30]	2006	0.7104	0.9740	0.9404	0.9436	0.7895
Line Detector[31]	2007	0.4966	0.9831	0.9212	0.8655	0.5590
SE[32]	2013	0.5309	0.9780	0.9211	0.8935	0.7767
Kernel Boost[33]	2013	0.7133	0.9810	0.9469	0.9307	0.7938
DeepVessel[21]	2016	0.7603	N.A	0.9523	N.A	N.A
Pixel CNN (Liskowski)[15]	2016	0.7811	0.9807	0.9535	0.9790	N.A
DRIU[20]	2016	0.7855	0.9799	0.9552	0.9793	0.7800
Patch FCN (Américo)[17]	2017	0.7810	0.9800	0.9543	0.9768	N.A
Patch FCN (Feng)[19]	2017	0.7811	<b>0.9839</b>	<b>0.9560</b>	0.9792	N.A
Image S-DSN (584×565)	2018	<b>0.7893</b>	0.9789	0.9547	0.9793	0.7843
Patch S-DSN (292×282)	2018	0.7890	0.9803	<b>0.9560</b>	<b>0.9802</b>	0.7980

<sup>1</sup> N.A = Not Available

## References

1. Karpecki, Paul, M.: Kanskis clinical ophthalmology: A systematic approach, 8th ed., brad bowling. *Optometry & Vision Science* **92** (2015)
2. Teng, T., Lefley, M., Claremont, D.: Progress towards automated diabetic ocular screening: A review of image analysis and intelligent systems for diabetic retinopathy. *Medical & Biological Engineering & Computing* **40**(1) (2002) 2–13
3. Haddouche, A., Adel, M., Rasigni, M., Conrath, J., Bourennane, S.: Detection of the foveal avascular zone on retinal angiograms using markov random fields. *Digital Signal Processing* **20**(1) (2010) 149–154
4. Kirbas, C.: A review of vessel extraction techniques and algorithms. *Acm Computing Surveys* **36**(2) (2004) 81–121
5. Fraz, M.M., Barman, S.A., Remagnino, P., Hoppe, A., Basit, A., Uyyanonvara, B., Rudnicka, A.R., Owen, C.G.: An approach to localize the retinal blood vessels using bit planes and centerline detection. *Computer Methods & Programs in Biomedicine* **108**(2) (2012) 600–616
6. Fraz, M.M., Remagnino, P., Hoppe, A., Uyyanonvara, B., Rudnicka, A.R., Owen, C.G., Barman, S.A.: Blood vessel segmentation methodologies in retinal images - a survey. *Computer Methods & Programs in Biomedicine* **108**(1) (2012) 407–33
7. Mo, J., Lei, Z.: Multi-level deep supervised networks for retinal vessel segmentation. *International Journal of Computer Assisted Radiology & Surgery* (9) (2017) 1–13
8. Azzopardi, G., Petkov, N.: Automatic detection of vascular bifurcations in segmented retinal images using trainable cosfire filters. *Pattern Recognition Letters* **34**(8) (2013) 922–933
9. Yin, Y., Adel, M., Bourennane, S.: Retinal vessel segmentation using a probabilistic tracking method. *Pattern Recognition* **45**(4) (2012) 1235–1244
10. Wang, L., Bhalerao, A., Wilson, R.: Analysis of retinal vasculature using a multiresolution hermite model. *IEEE Transactions on Medical Imaging* **26**(2) (2007) 137–52
11. Al-Diri, B., Hunter, A., Steel, D.: An active contour model for segmenting and measuring retinal vessels. *IEEE Transactions on Medical Imaging* **28**(9) (2009) 1488
12. Sum, K.W., Cheung, P.Y.: Vessel extraction under non-uniform illumination: a level set approach. *IEEE transactions on bio-medical engineering* **55**(1) (2008) 358–60
13. Emary, E., Zawbaa, H.M., Hassanien, A.E., Schaefer, G.: Retinal vessel segmentation based on possibilistic fuzzy c-means clustering optimised with cuckoo search. In: *International Joint Conference on Neural Networks*. (2014) 1792–1796
14. Melinsca, M., Prentasic, P., Loncaric, S.: Retinal vessel segmentation using deep neural networks. *Visapp* (2015)
15. Liskowski, P., Krawiec, K.: Segmenting retinal blood vessels with deep neural networks. *IEEE Transactions on Medical Imaging* **35**(11) (2016) 2369–2380
16. Khalaf, A.F., Yassine, I.A., Fahmy, A.S.: Convolutional neural networks for deep feature learning in retinal vessel segmentation. In: *IEEE International Conference on Image Processing*. (2016) 385–388
17. Oliveira, A., Pereira, S., Silva, C.A.: Augmenting data when training a cnn for retinal vessel segmentation: How to warp? In: *Bioengineering*. (2017) 1–4
18. Li, Q., Feng, B., Xie, L.P., Liang, P., Zhang, H., Wang, T.: A cross-modality learning approach for vessel segmentation in retinal images. *IEEE Transactions on Medical Imaging* **35**(1) (2016) 109

19. Feng, Z., Yang, J., Yao, L.: Patch-based fully convolutional neural network with skip connections for retinal blood vessel segmentation. (2017)
20. Maninis, K.K., Pont-Tuset, J., Arbeláez, P., Van Gool, L.: Deep retinal image understanding. In: International Conference on Medical Image Computing and Computer-Assisted Intervention, Springer (2016) 140–148
21. Fu, H., Xu, Y., Lin, S., Wong, D.W.K., Liu, J.: Deepvessel: Retinal vessel segmentation via deep learning and conditional random field. In: International Conference on Medical Image Computing and Computer-Assisted Intervention. (2016) 132–139
22. Xie, S., Tu, Z.: Holistically-nested edge detection. International Journal of Computer Vision (2015) 1–16
23. Long, J., Shelhamer, E., Darrell, T.: Fully convolutional networks for semantic segmentation. IEEE Transactions on Pattern Analysis & Machine Intelligence **39**(4) (2017) 640–651
24. Simonyan, K., Zisserman, A.: Very deep convolutional networks for large-scale image recognition. Computer Science (2014)
25. Lee, C.Y., Xie, S., Gallagher, P., Zhang, Z., Tu, Z.: Deeply-supervised nets. In: Artificial Intelligence and Statistics. (2015) 562–570
26. Jia, Yangqing, Shelhamer, Evan, Donahue, Jeff, Karayev, Sergey, Long, Jonathan: Caffe: Convolutional architecture for fast feature embedding. (2014) 675–678
27. Glorot, X., Bengio, Y.: Understanding the difficulty of training deep feedforward neural networks. Journal of Machine Learning Research **9** (2010) 249–256
28. Staal, J., Abramoff, M.D., Niemeijer, M., Viergever, M.A., Van Ginneken, B.: Ridge-based vessel segmentation in color images of the retina. IEEE transactions on medical imaging **23**(4) (2004) 501–509
29. Fan, D.P., Cheng, M.M., Liu, Y., Li, T., Borji, A.: Structure-measure: A new way to evaluate foreground maps. In: Proceedings of the IEEE Conference on Computer Vision and Pattern Recognition. (2017) 4548–4557
30. Soares, J.V., Leandro, J.J., Cesar, R.M., Jelinek, H.F., Cree, M.J.: Retinal vessel segmentation using the 2-d gabor wavelet and supervised classification. IEEE Transactions on medical Imaging **25**(9) (2006) 1214–1222
31. Ricci, E., Perfetti, R.: Retinal blood vessel segmentation using line operators and support vector classification. IEEE transactions on medical imaging **26**(10) (2007) 1357–1365
32. Dollár, P., Zitnick, C.L.: Structured forests for fast edge detection. In: Proceedings of the IEEE International Conference on Computer Vision. (2013) 1841–1848
33. Becker, C., Rigamonti, R., Lepetit, V., Fua, P.: Supervised feature learning for curvilinear structure segmentation. In: International Conference on Medical Image Computing and Computer-Assisted Intervention, Springer (2013) 526–533